New Journal of Physics
The open access journal at the forefront of physics

Deutsche Physikalische Gesellschaft DPG IOP Institute of Physics

PAPER • OPEN ACCESS

Type-II nodal line semimetal

To cite this article: Jing He *et al* 2018 *New J. Phys.* **20** 053019

New Journal of Physics
The open access journal at the forefront of physics

Deutsche Physikalische Gesellschaft DPG
IOP Institute of Physics

Published in partnership with: Deutsche Physikalische Gesellschaft and the Institute of Physics

OPEN ACCESS

RECEIVED
29 September 2017

REVISED
27 March 2018

ACCEPTED FOR PUBLICATION
13 April 2018

PUBLISHED
4 May 2018

PAPER

Type-II nodal line semimetal

Jing He[1,2], Xiao Kong[2], Wei Wang[2] and Su-Peng Kou[2]

[1] Department of Physics, Hebei Normal University, Shijiazhuang 050024, People's Republic of China
[2] Center for Advanced Quantum Studies, Department of Physics, Beijing Normal University, Beijing 100875, People's Republic of China

E-mail: spkou@bnu.edu.cn

Keywords: topological semimetal, magnetic order parameter, strongly correlation system

Abstract

Recently, topological semimetals have become a hot topic in condensed matter physics, including Dirac semimetals, Weyl semimetals, and nodal line semimetals (NLSMs). In this paper, a new type of NLSM—type-II NLSM—is proposed based on a two-band cubic lattice model. For type-II NLSM, the zero energy bulk states have a closed loop in momentum space but the (local) Weyl cones on the nodal line become tilted. The effect of the magnetic field and that of the correlation on type-II NLSM are studied. In particular, after considering the repulsive interaction and additional spin degrees of freedom, different types of long range magnetic orders appear in bulk states. In addition, the interaction-induced ferromagnetic (FM) order of surface states may exist. At a critical point between type-I NLSM and type-II NLSM, arbitrary tiny interactions induce FM order due to a flat band at the Fermi surface.

1. Introduction

Recently, topological semimetals have attracted considerable attention of researchers. Compared to topological insulators, topological semimetals have gapless bulk states and topologically protected surface Fermi arc states. There exist different types of topological semimetals, such as the Dirac semimetal (DSM) [1–3], Weyl semimetal (WSM) [4–7], and nodal line semimetal (NLSM) [8–11]. The WSM was proposed to separate a single Dirac node into two Weyl nodes by breaking either the time-reversal symmetry or inversion symmetry. The surface states of the WSM become a Fermi arc between a pair of Weyl points with opposite chiralities. Moreover, WSMs have been found in experiments such as the TaAs family [12–16]. NLSMs are a three-dimensional graphene-like system with low-energy relativistic excitations, but the band touches are closed loop in momentum space instead of points. The surface states of node-line semimetals have drumhead-like surface flat bands. The node-line semimetal is also realized in experiments (For example Ca_3P_2 [17]) and predicted by the first-principles calculation (For example Cu_3PdN [18]). In most topological materials, spin–orbit coupling plays important role. However, in some materials (for example, Cu_3PdN), there may exist a NLSM without spin–orbit coupling. After considering spin–orbital coupling, a nodal line could change into a pair of Weyl nodes and then the system becomes a WSM.

In addition, new types of WSMs are proposed which are called type-II WSM [19] and Hybrid (type-1.5) WSM [20, 21]. In these types of WSMs, Lorentz invariance of low-energy excitations is broken. As a result, the nodes are tilted along given directions (see figures 1(a) and (b)) and the transport properties become anisotropic. Many remarkable phenomena appear in type-II WSMs, such as the anisotropic negative magnetoresistance effect caused by Landau level collapse [22, 23] and the existence of tilted surface states [21]. In Hybrid (type-1.5) WSMs, because the remaining symmetry (inversion symmetry, time-reversal symmetry or mirror symmetry) of two nodes is broken, one Weyl node belongs to type-I and the other Weyl node belongs to type-II. These new types of WSMs have attracted plenty of attention in the past two years.

In this paper, based on a tight-binding model, we point out that there exists a new type of NLSM called *type-II NLSM*. Almost at the same time several analogous works are springing up. Theory and material realization have been put forward [24–27]. For type-II NLSM, the zero energy bulk states have a closed loop in momentum space but the (local) Weyl cones on the nodal line become tilted (see figures 1(c) and (d)). In sections 2 and 3, we

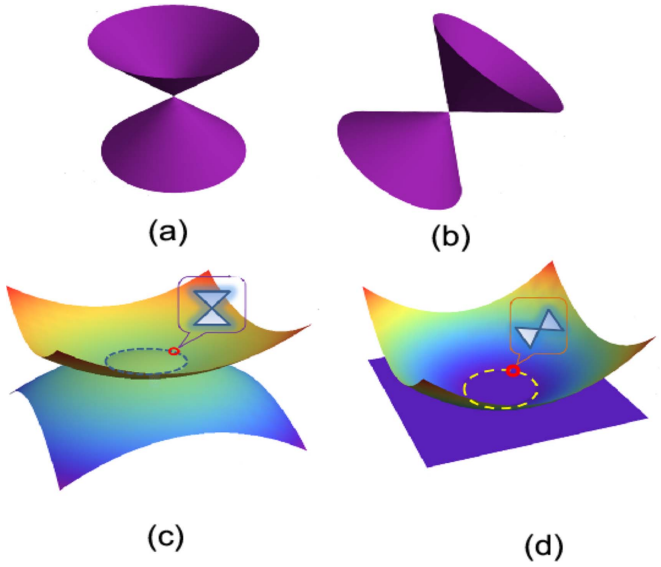

Figure 1. (a) An illustration of the low energy linear dispersion of type-I WSM. (b) An illustration of the low energy linear dispersion of the type-II WSM, which is tilted along a certain direction in the Brillouin zone (BZ). The electron and hole pockets touch, and the dispersions become anisotropic. (c) An illustration of the low energy dispersion of type-I NLSM that has a closed loop in momentum space. The low energy effective excitation of every node on the nodal line is also linear. (d) An illustration of the low energy dispersion of type-II NLSM that also has a closed loop in momentum space. Due to the tilted linear dispersion, the valence and conduction bands are asymmetry.

introduce a two-band tight-binding model that describes type-II NLSMs. In section 4, we study the effect of the magnetic field on type-II NLSMs and show the Landau level collapse in this system. Next, we study the correlation effect on type-II NLSMs and the interaction-induced magnetic order of NLSM is found in section 5. An interesting result is at the critical point between the type-I NLSM and type-II NLSM, arbitrary tiny interaction induces ferromagnetic order (FM) due to a flat band at the Fermi surface. Finally, we give a conclusion and propose an experimental realization in section 6.

2. The nodal line Hamiltonian in real space on a cubic lattice

Firstly, we start with a NLSM from a three-dimensional (3D) tight-binding Hamiltonian on a cubic lattice that is given by

$$\begin{aligned} H_0 = {} & t_{x/y/z}\sum_{i,a}(-1)^a(\hat{c}^{\dagger}_{i,a}\hat{c}_{i+\bar{\delta}_{1/2/3},a} + h.c.) \\ & - 2t_{xy}(1+\cos k_0)\sum_{i,a}(-1)^a\hat{c}^{\dagger}_{i,a}\hat{c}_{i,a} - 2t_{z0}\sum_{i,a}(-1)^a\hat{c}^{\dagger}_{i,a}\hat{c}_{i,a} \\ & + t'_{xz}\sum_{i}(\mathrm{e}^{-\mathrm{i}k_{x0}}\hat{c}^{\dagger}_{i,1}\hat{c}_{i+\bar{b}_1,2} + \mathrm{e}^{\mathrm{i}k_{x0}}\hat{c}^{\dagger}_{i,1}\hat{c}_{i-\bar{b}_1,2} \\ & - \mathrm{e}^{-\mathrm{i}k_{x0}}\hat{c}^{\dagger}_{i,1}\hat{c}_{i+\bar{b}_2,2} - \mathrm{e}^{\mathrm{i}k_{x0}}\hat{c}^{\dagger}_{i,1}\hat{c}_{i-\bar{b}_2,2} + h.c.) \\ & + t'_{yz}\sum_{i}(-\mathrm{i}\mathrm{e}^{-\mathrm{i}k_{y0}}\hat{c}^{\dagger}_{i,1}\hat{c}_{i+\bar{b}_3,2} - \mathrm{i}\mathrm{e}^{\mathrm{i}k_{y0}}\hat{c}^{\dagger}_{i,1}\hat{c}_{i-\bar{b}_3,2} \\ & + \mathrm{i}\mathrm{e}^{-\mathrm{i}k_{y0}}\hat{c}^{\dagger}_{i,1}\hat{c}_{i+\bar{b}_4,2} + \mathrm{i}\mathrm{e}^{\mathrm{i}k_{y0}}\hat{c}^{\dagger}_{i,1}\hat{c}_{i-\bar{b}_4,2} + h.c.) \end{aligned} \tag{1}$$

where $a = 1, 2$ is the orbital degrees of freedom. $\hat{c}_{i,a}$ is the annihilation operator of the electron at site i with an orbital degrees of freedom. $t_{x/y/z}$ are the nearest neighbor hoppings in $x/y/z$ direction, t'_{xz}/t'_{yz} are the orbital–flip hoppings in xoz/yoz plane. t_{xy}/t_{z0} are the effective Zeeman field. k_0 determines the radius of the nodal line. $k_{x0} = 0.4\pi, k_{y0} = 0.4\pi$ are to eliminate the Weyl points. $\bar{\delta}_{1/2/3}$ are the nearest vectors which are $(a_0, 0, 0)$, $(0, a_0, 0)$, $(0, 0, a_0)$, $\bar{b}_{1/2/3/4}$ are the next nearest vectors which are $(a_0, 0, a_0)$, $(a_0, 0, -a_0)$, $(0, a_0, a_0)$, $(0, a_0, -a_0)$. The lattice constant a_0 is set to be a unit. It is obvious that not only the inversion symmetry but also the time-reversal symmetry are broken.

Using the Fourier transformation, we obtain the Hamiltonian in momentum space

$$H_0 = \sum_{k} C^{\dagger}_{k}\mathcal{H}(\mathbf{k})C_k \tag{2}$$

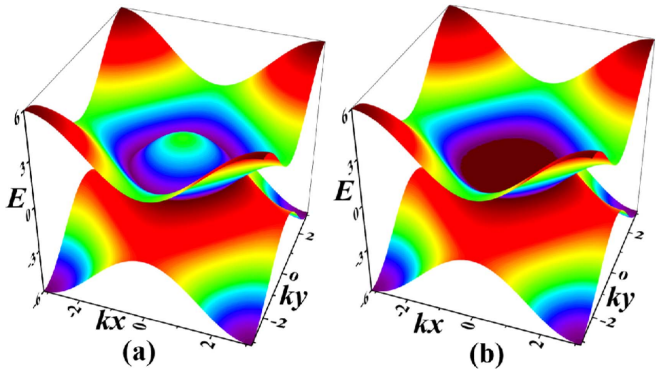

Figure 2. (a) The illustration of the nodal line located at the k_x–k_y plane for $k_z = 0$ with the radius of $k_0 = \pi/2$. (b) The surface states with periodic boundary conditions along the x- and y-direction but open boundary condition along the z-direction. There is a drumhead inside the nodal line. The parameters are $k_0 = \pi/2$, $t'_{xz} = t'_{yz} = 0.5t$.

with

$$\mathcal{H}(\mathbf{k}) = \vec{h}(\mathbf{k}) \cdot \hat{\sigma}, \tag{3}$$

where $C_k^\dagger = (C_{k,1}^\dagger, C_{k,2}^\dagger)$, $\hat{\sigma} = (\sigma_x, \sigma_y, \sigma_z)$ is the Pauli matrix, and $\vec{h}(\mathbf{k}) = (h_x(k), h_y(k), h_z(k))$ with

$$\begin{aligned} h_x(k) &= -4t'_{xz}\sin(k_x - k_{x0})\sin(k_z) \\ h_y(k) &= -4t'_{yz}\sin(k_y - k_{y0})\sin(k_z) \\ h_z(k) &= -2t_x\cos k_x - 2t_y\cos k_y - 2t_z\cos k_z \\ &\quad + 2t_{x/y}(1 + \cos k_0) + 2t_{z0}. \end{aligned}$$

Then, the spectrum for free fermions is derived as

$$E_{\mathbf{k},\pm} = \pm\sqrt{h_x^2(k) + h_y^2(k) + h_z^2(k)}. \tag{4}$$

In the following parts of the paper, the hopping parameters are set to $t_x = t_y = t_z = t_{xy} = t_{z0} = t$.

Next, we study the nodal line of the NLSM. In the k_x–k_y plane, the nodal line satisfies the equation of

$$\cos k_x + \cos k_y = 1 + \cos k_0. \tag{5}$$

Figure 2(a) shows the spectrum at $k_z = 0$. For this case, the nodal line is located at k_x–k_y plane with the radius of $k_0 = \pi/2$, $t'_{xz} = t'_{yz} = 0.5t$. This lattice model breaks the time-reversal and inversion symmetry. The stability of the nodal line protected by a particular 'mirror reflection' symmetry: a reflection with respect to the $z = 0$ mirror plane, and a two orbitals transformation as $\vec{h}(\mathbf{k}) \to (-h_x(k_x, k_y, -k_z), -h_y(k_x, k_y, -k_z), h_z(k_x, k_y, -k_z))$. Then the nodal line spectrum is protected by the mirror symmetry as $h_x = h_y = 0$ on the mirror plane.

To illustrate the topological properties of the NLSM, we calculate the Berry phases for a closed loop L in the momentum space not intersecting the nodal line as

$$P_B = \oint_L \mathbf{A}(\mathbf{k}) \cdot d\mathbf{k} \tag{6}$$

and $\mathbf{A}(\mathbf{k}) = -\mathrm{i}\langle\varphi(\mathbf{k})|\ \nabla_{\mathbf{k}}|\varphi(\mathbf{k})\rangle$, where $\mathbf{A}(\mathbf{k})$ is the Berry Connection and $\varphi(\mathbf{k})$ is the wavefunction of the ground state. After numerical calculations, we find that if the closed loop L is pierced by the nodal line, the Berry phase is $P_B = \pi$, for other cases, the Berry phase is $P_B = 0$. The nonzero Berry phases also signify the existence of flat surface states. Additionally, we also studied the surface state of the NLSM. We consider a system with periodic boundary conditions (PBC) along the x- and y-direction, but open boundary conditions (OBC) along the z-direction. By numerical calculations, the surface states are obtained in figure 2(b). Compared with figure 2(a), one can see that there exists a drumhead induced by the nodal line which is consistent with previous articles [18, 28], and the Fermi surface like disk in the core of the BZ.

3. Type-II NLSM

In this section, a new type of NLSM called the type-II NLSM is proposed. To get the typical type-II NLSM, we add a new term into the original model as

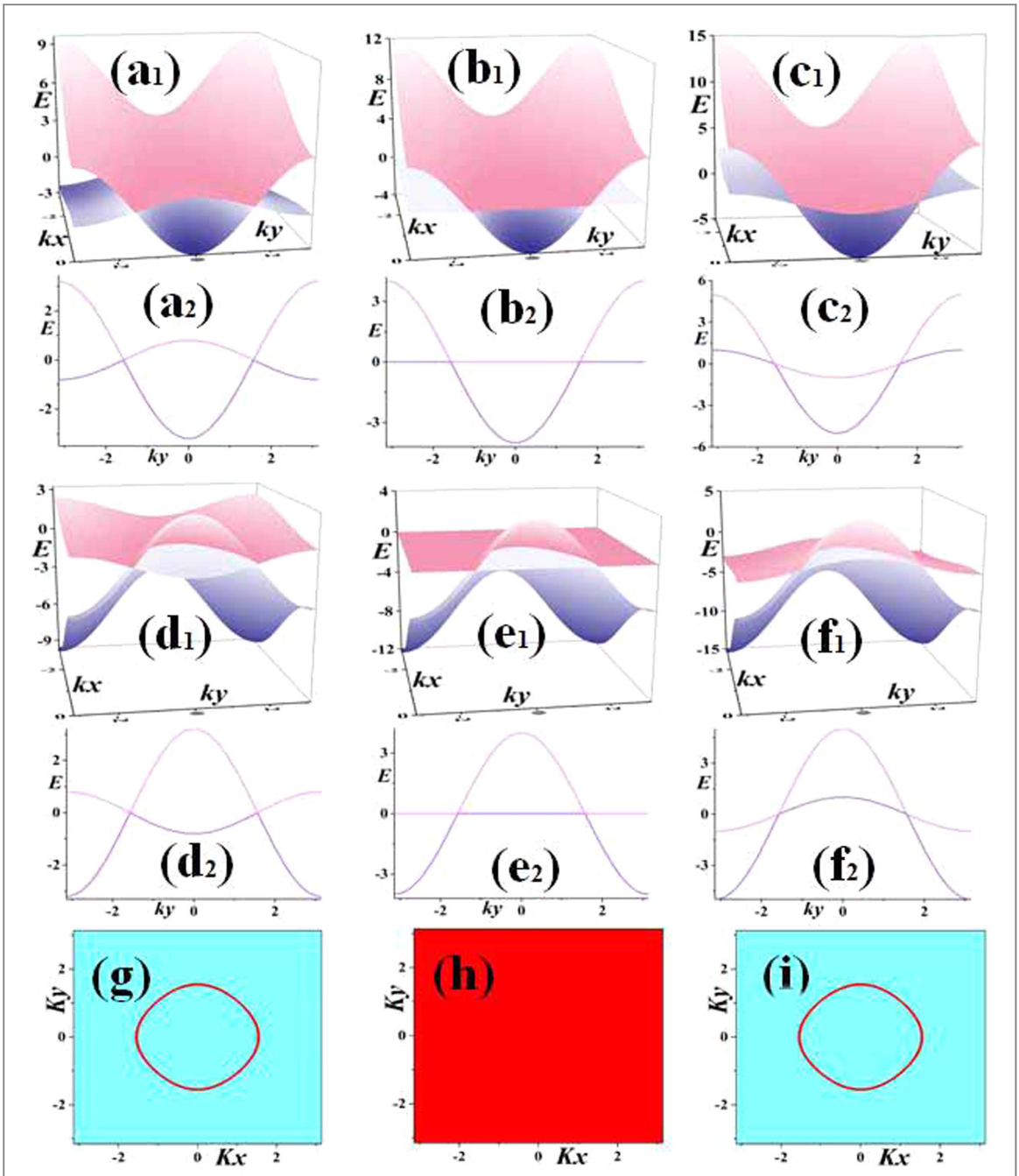

Figure 3. The dispersion of bulk states of the type-II NLSM. (*a*)–(*c*) $C = 0.6$, $C = 1.0$ and $C = 1.5$; (*d*)–(*f*) $C = -0.6$, $C = -1.0$ and $C = -1.5$. Subscripts 1 and 2 represent the 3D *E*–*k* dispersion and 2D *E*–*k* dispersion, 2D *E*–*k* dispersion is a planar cut of the **k**-space with $k_x = 0$. The tilting of the spectrums towards the center of the nodal line for the case of $C > 0$; while away from the center of the nodal line for the case of $C < 0$. There is a flat band Fermi surface when $|C| = 1$ in (*b*) and (*e*). For the case of $|C| > 1$, one of the energy bands reverses. (*g*)–(*i*) Fermi surface of the bulk system of $|C| = 0.6,\ 1.0$ and 1.5.

$$\mathcal{H}(\mathbf{k}) = \vec{h}(\mathbf{k}) \cdot \hat{\sigma} + h_0 I \tag{7}$$

with

$$h_0(k) = C[-2t_x \cos(k_x) - 2t_y \cos(k_y) + 2t_{x/y}(1 + \cos(k_0))] \tag{8}$$

C is a coefficient that determines the type of NLSM. $|C| = 1$ is a critical point: when $|C| < 1$, the NLSM belongs to the type-I NLSM; when $|C| > 1$, the NLSM belongs to the type-II NLSM. At the critical point $|C| = 1$, NLSM has a flat band at the Fermi surface, as figure 3(h) (the red region) shows. For the case of $|C| > 1$, one of the energy bands reverses.

The sign of coefficient C denotes the tilting orientation: when $C > 0$, the tilting of the spectra is towards the center of the node-line, while away from the center when $C < 0$. Numerical calculation of dispersions is shown in figure 3: the coefficient $C > 0$ for (*a*)–(*c*), while $C < 0$ for (*d*)–(*f*). The subscript 1 and 2 represents 3D *E*–*k* dispersion and 2D

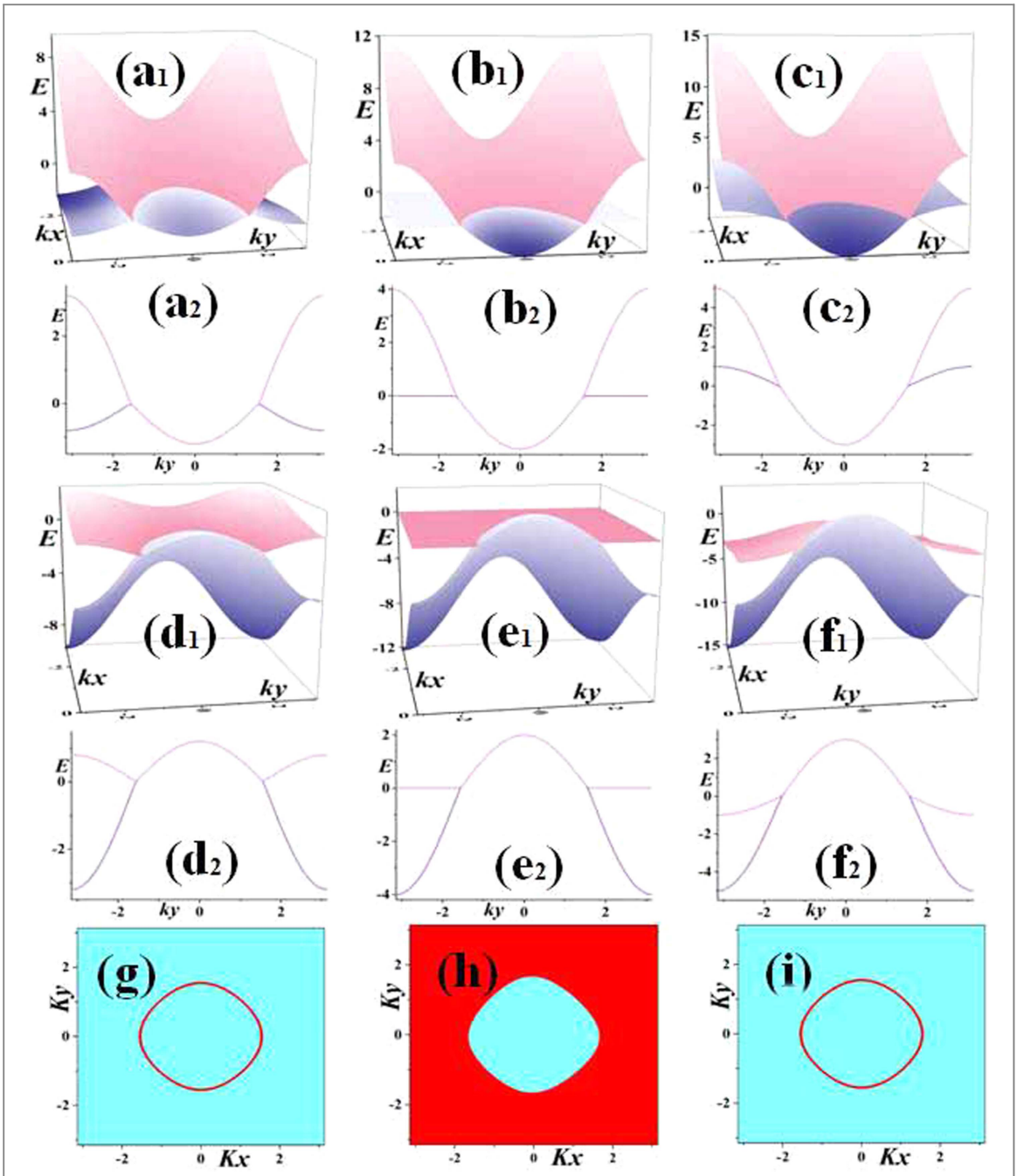

Figure 4. The dispersion of surface states for type-II NLSM. (*a*)–(*c*) $C = 0.6$, $C = 1.0$ and $C = 1.5$; (*d*)–(*f*) $C = -0.6$, $C = -1.0$ and $C = -1.5$. Subscripts 1 and 2 represent 3D *E*–*k* dispersion and 2D *E*–*k* dispersion, 2D *E*–*k* dispersion is a planar cut of the **k**-space with $k_x = 0$. Due to the existence of the tilting term of $C \neq 0$, the drumhead-like surface flat bands like in figure 2 (b) disappears. For the case of $|C| < 1$ ((*a*) and (*d*)), the Fermi surface is a circle (like (*g*)); at the critical point $|C| = 1$ ((*b*) and (*e*)), the Fermi surface changes into a flat band with a hole in the center (like (*h*)); for the case of $|C| > 1$ ((*c*) and (*f*)), the Fermi surface changes back into a circle one (like (*i*)).

E–*k* dispersion. 2D *E*–*k* dispersion is a planar cut of the **k**-space with $k_x = 0$. We can see clearly the tilting of the nodal line towards the center of the nodal line when $C > 0$; while away from the center when $C < 0$, (*g*)–(*i*) are the Fermi surface of the bulk system for $|C| = 0.6,\ 1.0$ and 1.5.

We then study the topological properties of type-II NLSM. The topological protected surface state is a hallmark of the topological system. In the type-II NLSM, the surface states show similar behavior of the nodal states on bulk systems—the surface states can also be tilted and become 'type-II'. In tilted NLSMs, the surface states are shown in figure 4, the top views from *z* axis for lowest two bands near the Fermi surface. In figure 4, the coefficient $C > 0$ is for (*a*)–(*c*), while $C < 0$ is for (*d*)–(*f*). The subscripts 1 and 2 represent 3D *E*–*k* dispersion and 2D *E*–*k* dispersion. 2D *E*–*k* dispersion is a planar cut of the **k**-space with $k_x = 0$. Due to the tilting effect for the $C \neq 0$ case, the drumhead-like surface flat band like in figure 2(b) disappears and is replaced by a dispersive one. Thus, the surface states in NLSMs can also be tilted like nodal line in bulk, which is similar to type-II WSMs [19].

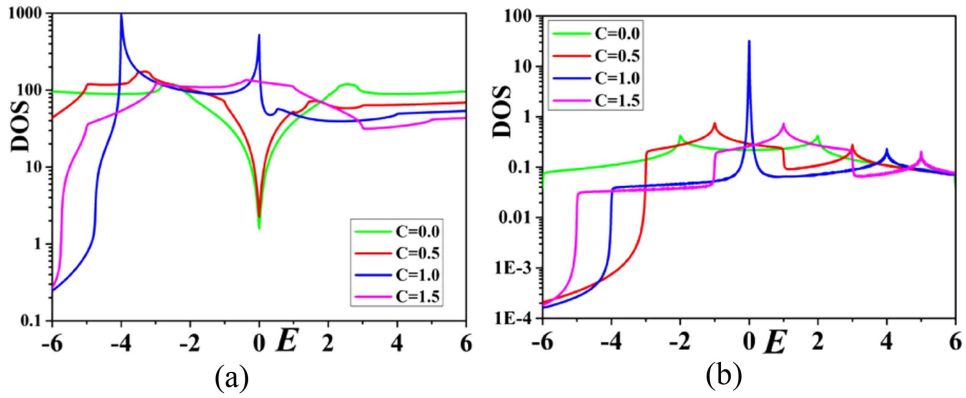

Figure 5. The DOS for type-II NLSMs. (*a*) For the whole BZ; (*b*) the DOS for $k_z = 0$ where the nodal line locates.

We discuss the evolution of the Fermi surface of lowest energy band of bulk states. In type-I NLSMs with $C = 0$, the Fermi surface of bulk states is a circle at $\mu = 0$ (here μ is the chemical potential). At the critical point $|C| = 1$, one band of the NLSM becomes flat, which leads to a tilted surface state. While the Fermi surface of the surface states is a disk at $\mu = 0$ when $C = 0$. At the critical point $|C| = 1$, it becomes a flat band with a hole in the center, like in figure 4(h).

In addition, we also calculate the density of states (DOS). The expression for calculating DOS is

$$\rho(\omega) = -\frac{1}{\pi}\,\mathrm{Im}\sum_{\sigma,k} G_\sigma(\omega,\, k),$$

where $G_\sigma(\omega,\, k)$ is Matsubara Green's Function which are

$$G_\uparrow(\omega,\, k) = \frac{|E_{\mathbf{k},\pm}| + h_z}{2|E_{\mathbf{k},\pm}|}\frac{1}{\omega + \mathrm{i}\eta - (h_0 + E_{\mathbf{k},+})} + \frac{|E_{\mathbf{k},\pm}| - h_z}{2|E_{\mathbf{k},\pm}|}\frac{1}{\omega + \mathrm{i}\eta - (h_0 + E_{\mathbf{k},-})}, \tag{9}$$

$$G_\downarrow(\omega,\, k) = \frac{|E_{\mathbf{k},\pm}| - h_z}{2|E_{\mathbf{k},\pm}|}\frac{1}{\omega + \mathrm{i}\eta - (h_0 + E_{\mathbf{k},+})} + \frac{|E_{\mathbf{k},\pm}| + h_z}{2|E_{\mathbf{k},\pm}|}\frac{1}{\omega + \mathrm{i}\eta - (h_0 + E_{\mathbf{k},-})}. \tag{10}$$

Here η is an infinite small quantity and real, ω is the energy level. After considering the tilting effect on the spectra, the DOS changes correspondingly. For $C = 0$, the spectrum and the DOS are symmetric; while for the cases of $C > 1$ and $C < 1$, the spectrum and the DOS are asymmetric. In particular, for $C > 1$, an energy band inverses. The Fermi surface of bulk states appears. As a result, for the DOS in the whole BZ, there is no peak at $E = 0$, like figure 5(a). In figure 5(b), for $k_z = 0$, owing to the existence of the bulk flat band, there exists a sharp peak at $E = 0$ for the case of $|C| = 1$.

4. Effect of magnetic field on type-II NLSMs

In type-II WSMs, the negative magnetic effect (NME) becomes anisotropic. The failure of the NME in the prescribed direction is caused by the collapse of the Landau level [23]. We now show that the collapse of the Landau level also appears in NLSMs.

We add the magnetic field along the x-direction, i.e., $\mathbf{B} = B\hat{x}$ and $\mathbf{A} = (0,\, Bz/2,\, -By/2)$, then use the usual Peierls substitutions $k_z \to \tilde{k}_z - \mathrm{e}By/2$, $k_y \to \tilde{k}_y + \mathrm{e}Bz/2$. We introduce the ladder operators

$$a^\dagger = \left[\hbar\partial_y + \mathrm{i}\hbar\partial_z - \left(\frac{\mathrm{e}By}{2} + \mathrm{i}\frac{\mathrm{e}Bz}{2}\right)\right],$$

$$a = \left[-(\hbar\partial_y - \mathrm{i}\hbar\partial_z) - \left(\frac{\mathrm{e}By}{2} - \mathrm{i}\frac{\mathrm{e}Bz}{2}\right)\right],$$

where $\tilde{k}_z = -\mathrm{i}\hbar\partial_z$, $\tilde{k}_y = -\mathrm{i}\hbar\partial_y$. These operators rise and fall with the Landau levels of free electrons as

$$a^\dagger|n,\, k_x\rangle = \sqrt{n+1}\,|n+1,\, k_x\rangle \tag{11}$$

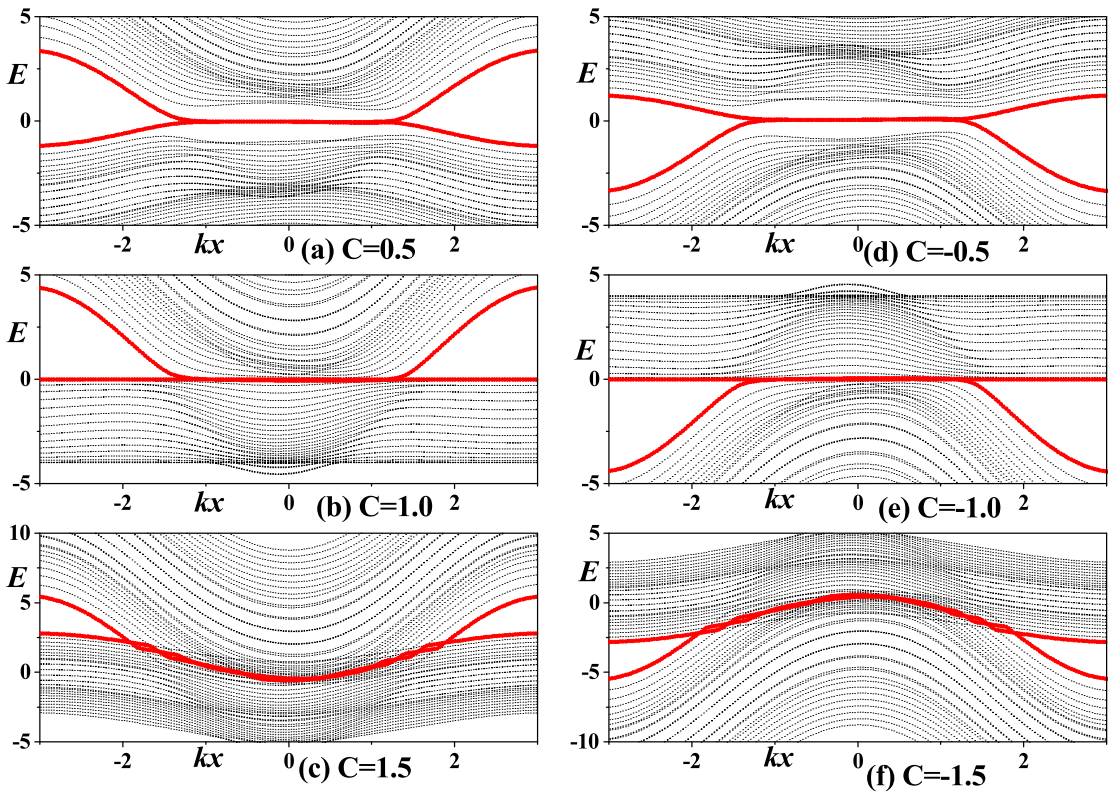

Figure 6. Dispersion of type-II NLSMs in a magnetic field along the x-direction with finite tilting strength.

and

$$a|n,\ k_x\rangle = \sqrt{n}\,|n-1,\ k_x\rangle, \tag{12}$$

where $|n,\ k_x\rangle$ is the free electron Landau level wavefunction. When an electron occupies the state $|n,\ k_x\rangle$, it rounds in circles in y–z plane. The translation invariance along the x-direction is preserved, so that k_x is still a good quantum number.

We expand the Hamiltonian near the nodal line and only keep the first-order terms, considering the perturbation along the radial (Δk_R) and tangential (Δk_T) directions of the nodal line. After a unitary transformation between two coordinates, we have

$$\Delta k_x \sigma_x + \Delta k_y \sigma_y = \Delta k_T \sigma_T + \Delta k_R \sigma_R$$

where $\sigma_T = \sigma_x \sin\theta - \sigma_y \cos\theta$, $\sigma_R = \sigma_x \cos\theta + \sigma_y \sin\theta$ and $k_T = k_x \sin\theta - k_y \cos\theta$, $k_R = k_x \cos\theta + k_y \sin\theta$, and θ is the intersection angle with the x-axis in x–y plane. Then, the Hamiltonian variation induced by the perturbation is

$$\begin{aligned}\Delta\mathcal{H}(\mathbf{k}) &= -2\Delta k_z(k_0\sigma_R + \Delta k_T\sigma_T + \Delta k_R\sigma_R)\\ &\quad + (2k_0\Delta k_R + \Delta k_z^2)\sigma_z + 2Ck_0\Delta k_R\sigma_0\\ &\simeq -2k_0\Delta k_z\sigma_R + 2k_0\Delta k_R\sigma_z + 2Ck_0\Delta k_R\sigma_0,\end{aligned} \tag{13}$$

which is independent of k_T because there is no dispersion along the nodal line. As a magnetic field is applied along the x-direction, and A_T (tangential directions of $\mathbf{A}$) is irrelevant, we focus on the tangential component of magnetic field $B\sin\theta$. The corresponding Landau levels near the nodal line become

$$E_{n\geqslant 1} = \pm v_0\sqrt{2n\alpha^3 e\hbar B\sqrt{1-(2k_x/\pi)^2}} \tag{14}$$

$$E_{n=0} = 0 \tag{15}$$

where $v_0 = 2k_0$, $\alpha = \sqrt{1-\beta^2}$, $\beta = C$, e is elementary charge, $\hbar$ is Planck constant. In the type-I region, the zeroth level $E = 0$ is maintained; in the type-II region $|C| > 1, 1-\beta^2 < 0$, so that α is imaginary and the expression is invalid. This corresponds to the collapse of the Landau levels mentioned in [23]. The zeroth Landau level also disappears.

In figure 6, we also give numerical results with different tilting strengths C. There are two flat bands near the nodal line when $|C| < 1$, which corresponds to the zeroth Landau level. When $|C| > 1$, the flat bands disappear, and the system becomes metal which is similar to WSMs [19–21].

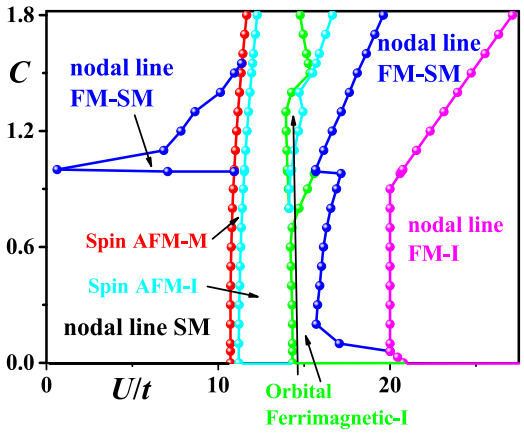

Figure 7. Global phase diagram for different tilting strengths C. There exist six phases: nodal line SM without any magnetic order, NLSM with FM order of spin degrees of freedom (FM–SM), metal with AF order of spin degrees of freedom (Spin AFM–M), insulator with AF order of spin degrees of freedom (Spin AFM–I), insulator with Ferrimagnetic order of orbital degrees of freedom (Orbital Ferrimagnetic-I) and nodal line insulator with FM order of spin degrees of freedom (FM–I). In the global phase diagram, there are three kinds of quantum phase transitions: one is between a long range ordered state and a phase without the long range order, the other is metal-insulator transition that is characterized by the zero fermion energy gaps, the third one is determined by the lower ground state energy.

5. Correlation effect on type-II NLSMs

In this section, we study the correlation effect on type-II NLSMs by considering an on-site repulsive interaction [29]. Then the Hamiltonian is rewritten as

$$H = H_{0,\uparrow} + H_{0,\downarrow} + U\sum_{i,a}\hat{n}_{i,\uparrow,a}\hat{n}_{i,\downarrow,a} - \mu\sum_{i,\tau,a}\hat{c}^{\dagger}_{i,\tau,a}\hat{c}_{i,\tau,a}, \tag{16}$$

where $H_{0,\uparrow}$ and $H_{0,\downarrow}$ are the Hamiltonians of equation (1) after considering the spin degrees of freedom. $\hat{n}_{i,\tau,a} = \hat{c}^{\dagger}_{i,\tau,a}\hat{c}_{i,\tau,a}$ is the operator of the particle number with two spin degrees of freedom τ and two orbital degrees of freedom a, U is the on-site Coulomb repulsive interaction strength and μ is the chemical potential.

Because the orbital SU(2) rotation symmetry is broken, when considering the repulsive interaction, the magnetic order of the spin degrees of freedom may appear and the corresponding spin SU(2) rotation symmetry is spontaneously broken. By the mean field theory, the FM order of spin degrees of freedom for bulk states is denoted by

$$\langle n_{i,\tau}\rangle = \frac{1}{2}(n + \tau M_{\mathrm{F}}), \tag{17}$$

where n is the number of particles, and we only consider the half-filling case for $n = 1$. $\tau = 1$ represents spin up and $\tau = -1$ represents spin down. M_{F} is the FM order parameter of spin degrees of freedom. We can write the self-consistent equations as

$$\langle n_{i\uparrow}\rangle + \langle n_{i\downarrow}\rangle = 1, \tag{18}$$

$$\langle n_{i\uparrow}\rangle - \langle n_{i\downarrow}\rangle = M_{\mathrm{F}}. \tag{19}$$

After the Fourier transformation, the self-consistent equations in momentum space can be rewritten as

$$M_{\mathrm{F}} = \frac{1}{2N}\sum_{k}[\theta(-E_{1\uparrow}) + \theta(-E_{2\uparrow}) - \theta(-E_{1\downarrow}) - \theta(-E_{2\downarrow})], \tag{20}$$

$$1 = \frac{1}{2N}\sum_{k}[\theta(-E_{1\uparrow}) + \theta(-E_{2\uparrow}) + \theta(-E_{1\downarrow}) + \theta(-E_{2\downarrow})], \tag{21}$$

where $\theta(x)$ is a step-up function and $\theta(x) = 1$ for $x > 0$ and $\theta(x) = 0$ for $x < 0$, N is the number of the unit cells and

$$E_{1\uparrow} = h_0 - \frac{UM_{\mathrm{F}}}{2} - \mu_{\mathrm{eff}} - E_{\mathbf{k}};$$

$$E_{2\uparrow} = h_0 - \frac{UM_{\mathrm{F}}}{2} - \mu_{\mathrm{eff}} + E_{\mathbf{k}};$$

$$E_{1\downarrow} = h_0 + \frac{UM_{\mathrm{F}}}{2} - \mu_{\mathrm{eff}} - E_{\mathbf{k}};$$

$$E_{2\downarrow} = h_0 + \frac{UM_{\mathrm{F}}}{2} - \mu_{\mathrm{eff}} + E_{\mathbf{k}},$$

with $\mu_{\mathrm{eff}} = \mu - \frac{U}{2}$.

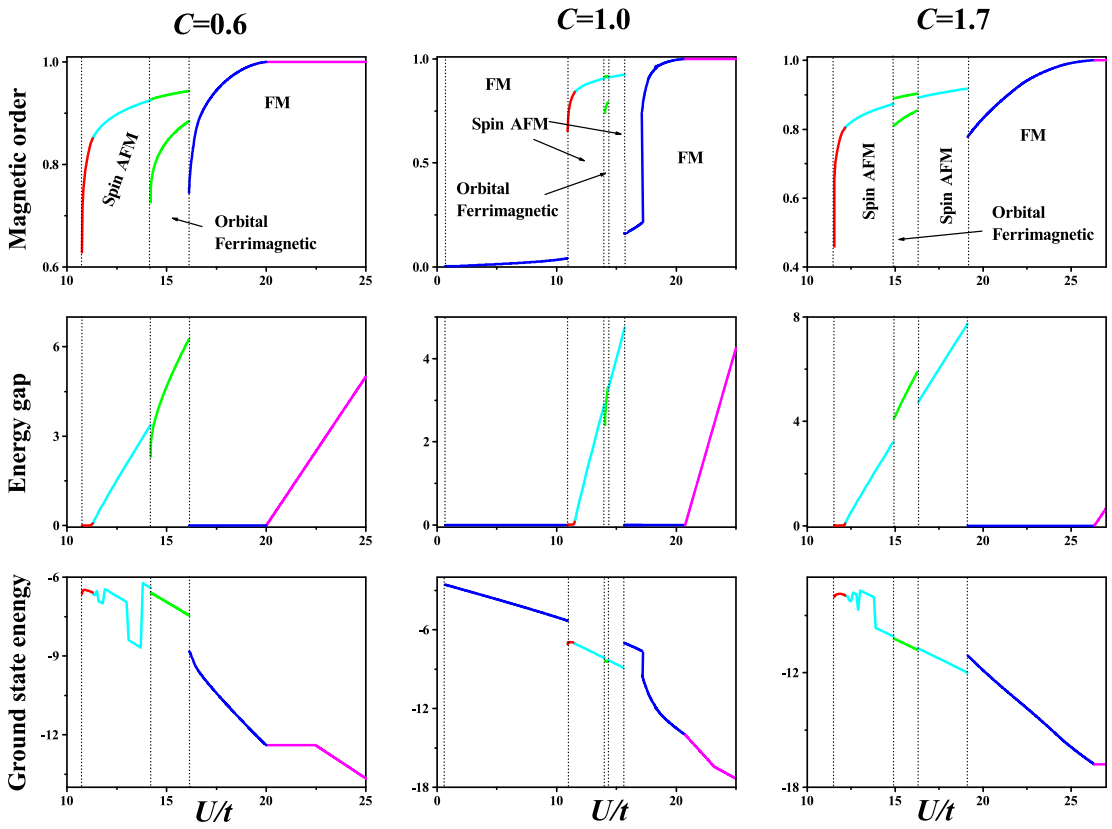

Figure 8. The first, second and third rows represent magnetization, the energy gap and the ground state energy, respectively. Different columns represent different tilting strengths. In these figures, we use different colored lines to represent different phases, the blue line represents nodal line FM-SM, the red line represents Spin AFM–M, the cyan line represents Spin AFM–I, the green line represents Orbital Ferrimagnetic-I and the magenta line represents nodal line FM–I. We use black dotted lines to distinguish the different magnetic order phases.

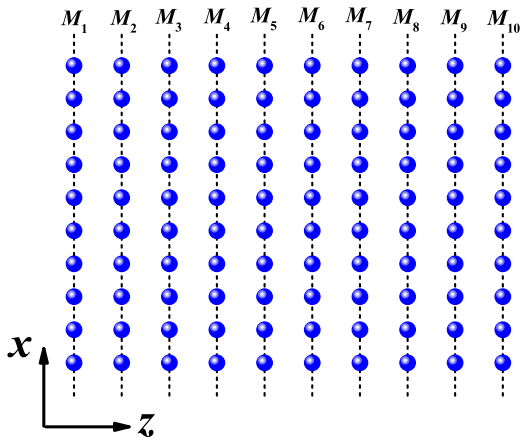

Figure 9. The illustration of the OBC for correlated effect on surface states. The system with PBC along the x- and y-direction, but OBC along the z-direction. M_1–M_{10} are FM orders for different levels of system.

At the mean field level, we can also define other long range orders: the antiferromagnetic (AF) order of spin degrees of freedom for bulk states

$$\langle n_{i,\tau}\rangle = \frac{1}{2}[n + (-1)^i \tau M_{\mathrm{AF}}] \tag{22}$$

where M_{AF} is the AF order parameter of spin degrees of freedom; the FM order of orbital degrees of freedom for bulk states

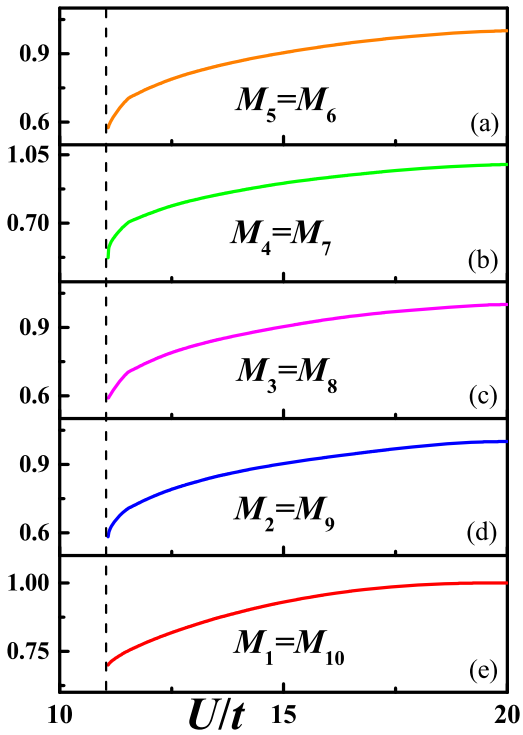

Figure 10. The FM order M of the system with OBC for the case of $C = 0.1$. The black dashed line represents the magnetic phase transition from $M = 0$ to $M \neq 0$. (*a*)–(*e*) are the FM orders of different sites. One can see that the surface FM order is more robust than the bulk FM order.

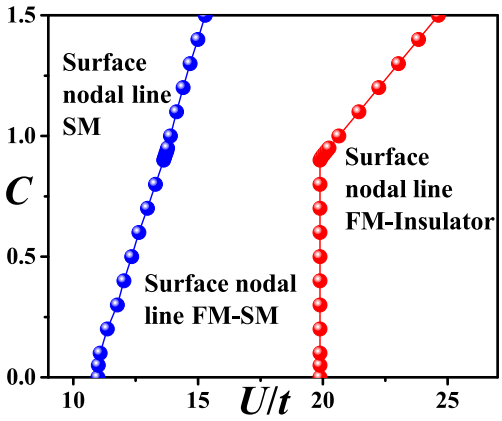

Figure 11. Global phase diagram for different tilting strengths C on surface states of NLSMs. There are three phases: surface NLSM without any magnetic order, surface NLSM with FM order of spin degrees of freedom (FM–SM), and surface nodal line insulator with FM order of spin degrees of freedom (FM–insulator). There are two phase transitions: the magnetic phase transition and the metal-insulator phase transition.

$$\langle n_{i,a}\rangle = \frac{1}{2}[n + (-1)^a M'_{\mathrm{F}}] \tag{23}$$

where M'_F is FM order parameter of orbital degrees of freedom; the AF order of orbital degrees of freedom for bulk states

$$\langle n_{i,a}\rangle = \frac{1}{2}[n + (-1)^i(-1)^a M'_{\mathrm{AF}}] \tag{24}$$

where M'_{AF} is AF order parameter of orbital degrees of freedom. These numerical calculations are the same as the FM case of spin degrees of freedom.

Then by using the mean field approach, we obtain the global phase diagram for different NLSMs with different tilting strengths C in figure 7. In figure 7, there exist six phases: nodal line SM without any long range order, NLSM with FM order of spin degrees of freedom (FM–SM), metal with AF order of spin degrees of

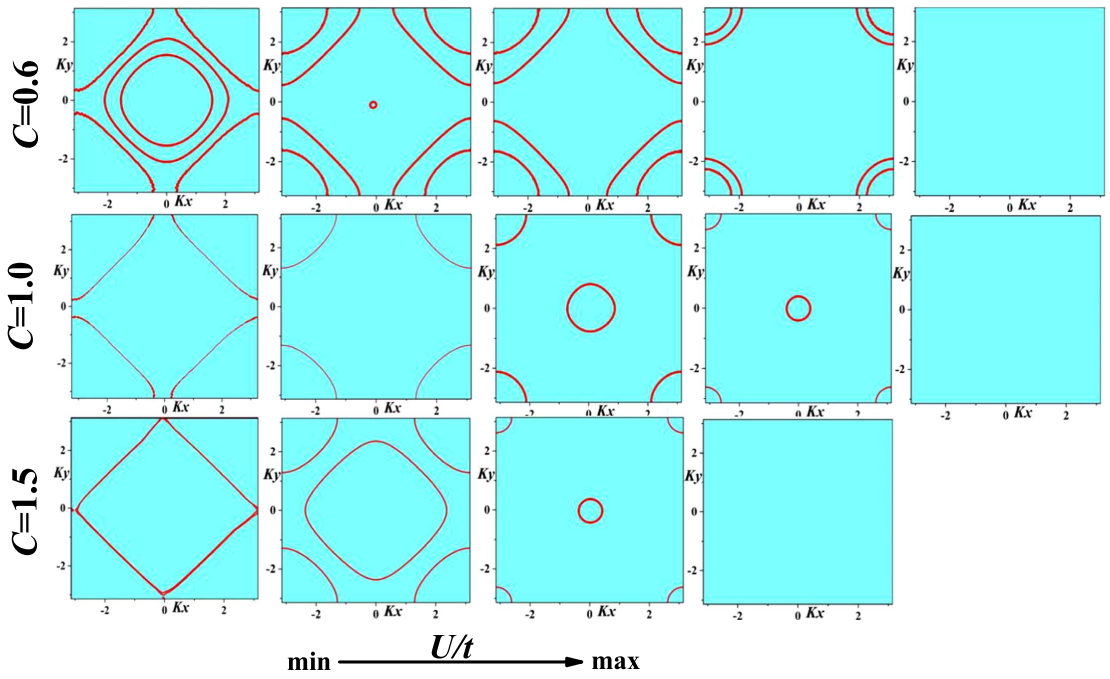

Figure 12. Fermi surface for surface states with different tilting strength C.

freedom (Spin AFM–M), insulator with AF order of spin degrees of freedom (Spin AFM–I), insulator with Ferrimagnetic order of orbital degrees of freedom (Orbital Ferrimagnetic-I) and nodal line insulator with FM order of spin degrees of freedom (FM–I). In the global phase diagram, there are three kinds of quantum phase transitions: the one is between a long range ordered state and a phase without the long range order, the other is a metal-insulator transition that is characterized by the zero fermion energy gaps, the third one is determined by the lower ground state energy.

In the global phase diagram, a remarkable result is found about the magnetic phase transition at $C = 1$. For the case of $C = 1$, there exists a flat band Fermi surface (see figure 3(h)). As a result, a very tiny repulsive interaction will induce an FM order of spin degrees of freedom (See the result in figure 7). In figure 8, we also plot the magnetization, the energy gap and the ground state energy via the repulsive interaction for the cases $C = 0.6$, $C = 1.0$ and $C = 1.7$, respectively. The first, second and third rows represent magnetization, the energy gap and the ground state energy, respectively. Different columns represent different tilting strengths. In these figures, we use different colored lines to represent different phases, the blue line represents nodal line FM-SM, the red line represents Spin AFM–M, the cyan line represents Spin AFM–I, the green line represents Orbital Ferrimagnetic-I and the magenta line represents nodal line FM–I. We use black dotted lines to distinguish the different magnetic order phases.

Next, we consider the correlated effect on surface states and show the interaction-induced surface orders in NLSMs. Because the orbital SU(2) rotation symmetry is broken and the AF order of spin degrees of freedom for surface states is not well defined, we focus on the FM order of spin degrees of freedom for surface states.

Because the nodal line locates at k_x–k_y plane, we consider a system with PBC along the x- and y-direction, but OBC along the z-direction. Now, due to SU(2) spin rotation symmetry, the ansatz of the FM order of spin degrees of freedom is the same as equation (17). Along the z-direction, the system has 10 lattice sites like in figure 9. Because there is no translation symmetry along the z-direction, we must calculate the mean field ansatz of FM order site-by-site. After considering inverse symmetry, there are five different cases to calculate. In figures 10(a)–(e) are the FM orders on different lattice sites along the z-direction.

After numerical calculations, we obtain the global phase diagram for different types of NLSMs with OBC in figure 11. Compared with figure 7, there exists three phases: surface NLSM without any magnetic order, surface NLSM with FM order of spin degrees of freedom (FM–SM), and surface nodal line insulator with FM order of spin degrees of freedom (FM–insulator). There are two phase transitions: the magnetic phase transition and the metal-insulator phase transition. Due to the effect of OBC, the results are different from figure 7. When we tune the strength of the repulsive interaction, the bulk FM order appears earlier than the surface FM order for different types of NLSMs.

Beyond the critical tilting point $C = 1$, one of the energy bands of surface states reverses. See figure 12. For different tilting strengths, with the increase of interaction, the shape of the Fermi surface for surface states changes, and finally the system becomes an insulator.

6. Conclusion

In this paper, we pointed out that there exists a new type of NLSM—type-II NLSM—based on a two-band cubic lattice model. We studied the effect of a magnetic field on type-II NLSM and found the Landau level collapses in this system. After considering repulsive interaction and additional spin degrees of freedom, different magnetic orders appear in the bulk states and FM order exists in surface states. At a critical point between the type-I NLSM and type-II NLSM, a arbitrary tiny interaction induces the FM order due to a flat band at the Fermi surface.

Finally, we propose an experimental setup to realize the NLSM on optical lattice. The model discussed in this paper includes complex-valued nearest and next nearest neighbor hopping in cubic lattice. Hopefully this can be realized in a three-dimensional optical lattice with two components of Fermi atoms such as ^{6}Li and ^{40}K. The real-valued hopping can be induced by kinetics which could be tuned by changing the potential depth and the imaginary-valued hopping could be induced by a two-photon Raman process or shaking lattice. A similar system in one dimension and two dimension had been realized recently [30, 31].

Acknowledgments

This work is supported by NSFC Grant No. 11174035, 11474025, 11404090, Natural Science Foundation of Hebei Province (Grant No. A2015205189), Hebei Education Department Natural Science Foundation (Grant No. QN2014022), SRFDP and distinguished young scholars of Hebei Normal university (Grant No.L2018J03).

ORCID iDs

Su-Peng Kou https://orcid.org/0000-0003-2225-3677

References

[1] Wang Z, Sun Y, Chen X Q, Franchini C, Xu G, Weng H, Dai X and Fang Z 2012 *Phys. Rev.* B **85** 195320
[2] Wang Z, Weng H, Wu Q, Dai X and Fang Z 2013 *Phys. Rev.* B **88** 125427
[3] Heikkila T and Volovik G E 2011 *JETP Lett.* **93** 59
[4] Nielsen H B and Ninomiya M 1983 *Phys. Lett.* **130B** 389
[5] Wan X, Turner A M, Vishwanath A and Savrasov S Y 2011 *Phys. Rev.* B **83** 205101
[6] Xu G, Weng H, Wang Z, Dai X and Fang Z 2011 *Phys. Rev. Lett.* **107** 186806
[7] Balents L 2011 *Physics* **4** 36
[8] Burkov A A, Hook M D and Balents L 2011 *Phys. Rev.* B **84** 235126
[9] Weng H, Liang Y, Xu Q, Yu R, Fang Z, Dai X and Kawazoe Y 2015 *Phys. Rev.* B **92** 045108
[10] Lim L K and Moessner R 2017 *Phys. Rev. Lett.* **118** 016401
[11] Fang C, Weng H M, Dai X and Fang Z 2016 *Chin. Phys.* B **11** 117106
[12] Xu S Y *et al* 2015 *Science* **349** 613
[13] Lv B Q *et al* 2015 *Phys. Rev.* X **5** 031013
[14] Lv B Q *et al* 2015 *Nat. Phys.* **11** 724
[15] Chang T R *et al* 2016 *Nat. Commun.* **7** 10639
[16] Xu N *et al* 2016 (arXiv: cond-mat/1604.02116)
[17] Xie L S, Schoop L M, Seibel E M, Gibson Q D, Xie W and Cava R J 2015 *APL Mater.* **3** 083602
[18] Yu R, Weng H M, Fang Z, Dai X and Hu X 2015 *Phys. Rev. Lett.* **115** 036807
[19] Soluyanov A A, Gresch D, Wang Z, Wu Q, Troyer M, Dai X and Bernevig B A 2015 *Nature* **527** 495
[20] Li F Y, Luo X, Dai X, Yu Y, Zhang F and Chen G 2016 *Phys. Rev.* B **94** 121105(R)
[21] Kong X, Ying J H L and Kou S P 2017 *Phys. Rev.* A **95** 033629
[22] Wang Y J *et al* 2016 *Nat. Commun.* **7** 13142
[23] Yu Z M and Yao Y G 2016 *Phys. Rev. Lett.* **117** 077202
[24] Li S, Yu Z M, Liu Y, Guan S, Wang S S, Zhang X M, Yao Y G and Yang S A 2017 *Phys. Rev.* B **96** 081106
[25] Zhang X M, Jin L, Dai X F and Liu G D 2017 *J. Phys. Chem. Lett.* **8** 4814–9
[26] Hyart T and Heikkila T T 2016 *Phys. Rev.* B **93** 235147
[27] Xu Y, Zhang F and Zhang C W 2015 *Phys. Rev. Lett.* **115** 265304
[28] Kim Y, Wieder B J, Kane C L and Rappe A M 2015 *Phys. Rev. Lett.* **115** 036806
[29] Roy B 2017 *Phys. Rev.* B **96** 041113
[30] Lin Y J, Jiménez-García K and Spielman I B 2011 *Nature* **471** 83–6
[31] Wu Z, Zhang L, Sun W, Xu X T, Wang B Z, Ji S C, Deng Y J, Chen S, Liu X J and Pan J W 2016 *Science* **354** 6308